Shap. Mem. Superelasticity
https://doi.org/10.1007/s40830-024-00497-7

ORIGINAL RESEARCH ARTICLE

On the Mechanisms and Thermocyclic Stability of $\beta \rightarrow \omega_{iso}$ Transformation in a Superelastic Ti–Nb–Zr Shape Memory Alloy

Alexandra Baranova[1] · Sergey Dubinskiy[1] · Anton Konopatsky[2] · Galina Markova[3] · Irina Vvedenskaia[1] · Sergey Prokoshkin[1] · Vladimir Brailovski[4]

Received: 29 February 2024 / Revised: 17 June 2024 / Accepted: 18 July 2024

Abstract The role of diffusion in the isothermal ω-phase formation and the $\beta \rightarrow \omega_{iso}$ transformation stability (reproducibility) during thermal cycling of a superelastic Ti–Nb–Zr shape memory alloy remain insufficiently studied. The distribution of chemical elements in the vicinity of ω_{iso}-phase particles after aging at 300 and 375 °C and the stability of $\beta \rightarrow \omega_{iso} \rightarrow \beta$ transformation in a heating half-cycle during thermal cycling of Ti–22Nb–6Zr (at. %) alloy were studied using high-resolution scanning transmission electron microscopy with energy dispersive X-ray spectroscopy techniques and X-ray diffractometry. It was shown that the leading mechanism of ω_{iso}-phase formation in the Ti–22Nb–6Zr alloy is a crystal lattice shear, while the diffusional redistribution of elements in the vicinity of ω_{iso}-phase particles plays a secondary role which appears only at higher aging temperatures. The $\beta \rightarrow \omega_{iso} \rightarrow \beta$ transformation features, β- and ω-phases structure parameters are stable and reproducible during thermal cycling up to at least ten cycles.

Keywords Titanium alloys · Shape memory alloys · $\beta \rightarrow \omega$ transformation mechanism · Lattice parameters · Thermal cycling · Aging

✉ Sergey Dubinskiy
sdubinskiy@gmail.com

[1] Present Address: National University of Science and Technology MISIS, 4 Leninskiy prospect, Moscow, Russia

[2] CRISMAT, CNRS, Normandie Univ, ENSICAEN, UNICAEN, 14000 Caen, France

[3] Tula State University, 92 Lenina prospect, Tula, Russia

[4] Ecole de Technologie Superieure, 1100 Notre-Dame Street West, Montreal, Canada

Introduction

Ti–Nb–Zr shape memory alloys (SMA) are promising materials for biomedical applications due to their excellent manufacturability and biocompatibility [1–9]. Their most important mechanical characteristic is the low Young's modulus (< 50 GPa), which ensures their biomechanical compatibility with bone tissue [3, 10–12] and non-linear superelastic behavior [8, 9]. The superelasticity of titanium SMA is based on the reversible thermoelastic martensitic transformation of the parent BCC β-phase into the martensitic orthorhombic α''-phase [13]. To improve the superelastic behavior, it is very important to obtain in these alloys the largest difference between the dislocation and transformation yield stresses for a more complete implementation of the stress-induced $\beta \leftrightarrow \alpha''$ martensitic transformation without involving irrecoverable true plastic deformation [14–20]. One of the ways to improve superelastic behavior is dispersion hardening of the alloys by aging due to the precipitation of ω-phase particles [13, 21, 22]. Dispersion hardening is of particular interest, since it does not require the use of plastic deformation and can be used for foam materials or complex structures or even devices obtained by additive manufacturing [23, 24]. Today, the ω-phase is classified into isothermal phase (ω_{iso}) [25, 26] formed during isothermal holding (aging), athermal phase (ω_{ath}) [27, 28] formed during cooling (quenching), and deformation phase (ω_{def}) formed under the influence of external stress [29, 30].

It was shown earlier that the precipitation of isothermal ω_{iso}-phase has C-shaped kinetics and is very sensitive to the "initial" internal stress level providing preferable sites for the ω_{iso}-phase formation and to the cooling-heating rate and direction of approach to the precipitation temperature range [31]. It was reported in [32, 33] that the ω_{iso}-phase formation

Published online: 01 August 2024

in some β-type alloys is accompanied by the redistribution of elements through the ω_{iso}-phase particle boundaries, however, the initial (embryonic) stage of the ω_{iso}-phase formation is a diffusionless process [33]. However, recent results in [31] exhibit a predominant role of shear mechanism of $\beta \rightarrow \omega_{iso}$ transformation in the Ti–22Nb–6Zr (at.%) alloy and a marginal role of the diffusion-related mechanisms. However, there is no direct evidence of how the diffusion phenomenon affects chemical composition of the β-phase matrix in the Ti–22Nb–6Zr alloy. Thus, a contribution of the diffusional mechanisms to the ω_{iso}-phase formation under different aging conditions remains unclear. It is important to bear in mind that the proven absence of diffusional redistribution of elements across the β/ω interface during the formation of the ω_{iso}-phase would indicate the shear nature of this process, as in the case of the formation of the athermal ω_{ath}-phase. We also note that during heating of the same alloy, $\beta \rightarrow \omega_{iso} \rightarrow \beta$ transformation occurred, while this transformation was not detected during subsequent cooling [34, 35], that brings attention to the ω_{iso}-phase formation thermocycling stability: repeatability upon repeatable heating–cooling cycles. The repeatability of the $\beta \rightarrow \omega_{iso}$ transformation is very important for the practical application of the recently discovered atypical Elinvar effect in Ti–22Nb–6Zr SMA [34]. An in-depth understanding of the $\beta \rightarrow \omega_{iso}$ transformation mechanism is an important factor in controlling the functional properties of Ti–22Nb–6Zr alloys used as shape memory alloys and Elinvar materials.

Thus, the aim of this work was to study the role of the element diffusion in the process of ω_{iso}-phase formation and impact of this phenomenon on the $\beta \rightarrow \omega_{iso}$ transformation thermocycling stability in Ti–22Nb–6Zr SMA.

Experimental

An 8 kg Ti–22Nb–6Zr (at.%) ingot was produced by vacuum-arc melting in *DVV-125* furnace, hot forged (*I.P. Bardin Central Research Institute of Ferrous Metallurgy*, Russia) and homogenized at 1100 °C for 30 min. The ingot had a low impurity content of O < 0.05, C < 0.01, N < 0.01, H < 0.01 (wt. %). After homogenization annealing, the ingot was EDM-cut into 20 × 10 × 50 (mm) billets, cold-rolled with a true strain of $e = 0.3$ and annealed at 600 or 750 °C for 30 min to form in this alloy a polygonized dislocation substructure (P state) or recrystallized structure (R state) states of β-phase, respectively [36]. For the Ti–22Nb–6Zr alloy, the polygonized dislocation substructure provided an optimal combination of functional properties [18, 37–39], such as recovery strain and lifetime under severe conditions of cyclic tensile tests. The recrystallized structure of the β-phase provided a state with a small number of crystal lattice defects commonly used as a reference treatment [38]. Then thermomechanically treated billets were aged at 300 or 375 °C for 3 h and water-cooled. The choice of aging temperatures was based on the following considerations about the ω_{iso}-phase formation: (1) 300 °C corresponds to the most intense ω_{iso}-phase formation during isothermal holding obtained in the study of C-shape kinetics [31]; and (2) 375 °C corresponds to the conditions under which the diffusion mobility of elements is increased while the ω-phase dissolution has not yet begun [34].

The structure and the phase composition after aging at 300 and 375 °C (3 h) with subsequent water-cooling were studied using a transmission electron microscope *JEOL JEM-2100* at 200 kV. Then an *FEI Technai Osiris* high-resolution scanning transmission electron microscope (STEM) equipped with the *SuperX* EDX system at 200 keV was used to study the distribution of chemical elements in areas surrounding the ω_{iso}-phase particles in the polygonized Ti–22Nb–6Zr alloy. The energy dispersive X-ray spectroscopy linear scanning analysis was performed with 0.4 nm step and 0.3 nm beam width. Both studies were carried out using 80–100 nm thick lamellas cut by the focused ion beam method on a *Strata FIB 205*.

To determine the statistical significance of the obtained differences in the Ti and Nb concentrations in the β-phase matrix, inside and around ω-phase particle, the statistical Student's test was used with an average significance level of 0.05 for the entire scanned range and separate ranges corresponding to the matrix and the particle. The mean values of Ti and Nb concentrations in each studied range were calculated using the Eq. (1):

$$\bar{x} = \frac{\sum_i x_i}{n}, \tag{1}$$

where x_i is the Ti or Nb concentrations in ith point of a given range and n is the number of measurements in this range. The standard deviation was calculated using the Eq. (2):

$$\sigma = \sqrt{\frac{\sum_i \left(\bar{x} - x_i\right)^2}{n}}. \tag{2}$$

The absolute confidence error was calculated using the Eq. (3):

$$\Delta = t_{P,k} \times \frac{\sigma}{\sqrt{n}}, \tag{3}$$

where $t_{P,k}$ is the critical values of the Student's coefficient for the confidence probability $P = 0.95$ and the number of freedom degrees $k = n - 1$.

To assess stability of the phase state after heating–cooling cycles and after water quenching from the characteristic temperatures reached on heating to 250, 375, and 550 °C in accordance with [34],

a room-temperature X-ray diffraction analysis was carried out for the 1st, 4th, and 10th heating–cooling cycles (Fig. 1) using a *DRON-4* diffractometer with $Cu_{K\alpha}$ radiation on $8 \times 10 \times 1 \ldots 2$ mm specimens. The average heating–cooling rate before quenching from the characteristic temperatures was ~ 2.5 °C/min. Before studies, the specimen surfaces were grinded with P320–P1200 abrasive paper and chemically etched in 1HF: $3HNO_3$: $6H_2O$ solution to remove the oxidized and mechanically damaged surface. The β-phase lattice parameter was calculated using the *Nelson–Riley* extrapolation. The lattice parameters of ω_{iso}-phase were calculated by the least-squares method previously used in [39]. The width of $\{110\}_\beta$ and $\{211\}_\beta$ X-ray line profiles was measured at half the height of the profile peak (half-height line width).

Results and Discussion

Study of $\beta \rightarrow \omega_{iso}$ Transformation Mechanism

To answer the question whether the diffusional redistribution of elements contributes to the $\beta \rightarrow \omega_{iso}$ transformation, the distribution of Ti, Nb, and Zr compositions across the ω-phase particles and in the β-phase areas surrounding the ω-phase particles were studied after aging at 300 and 375 °C (3 h) of an annealed at 600 °C, 30 min Ti–22Nb–6Zr alloy were studied. Figure 2 shows the TEM bright and dark field images of the alloy microstructure after aging, along with the corresponding SAED patterns.

After aging at both temperatures, elongated ω_{iso}-phase particles are formed, which is consistent with data of [26, 31]. This could indirectly indicate that the $\beta \rightarrow \omega$ transformation is predominantly initiated by the shear mechanism. Otherwise in case of diffusion controlled

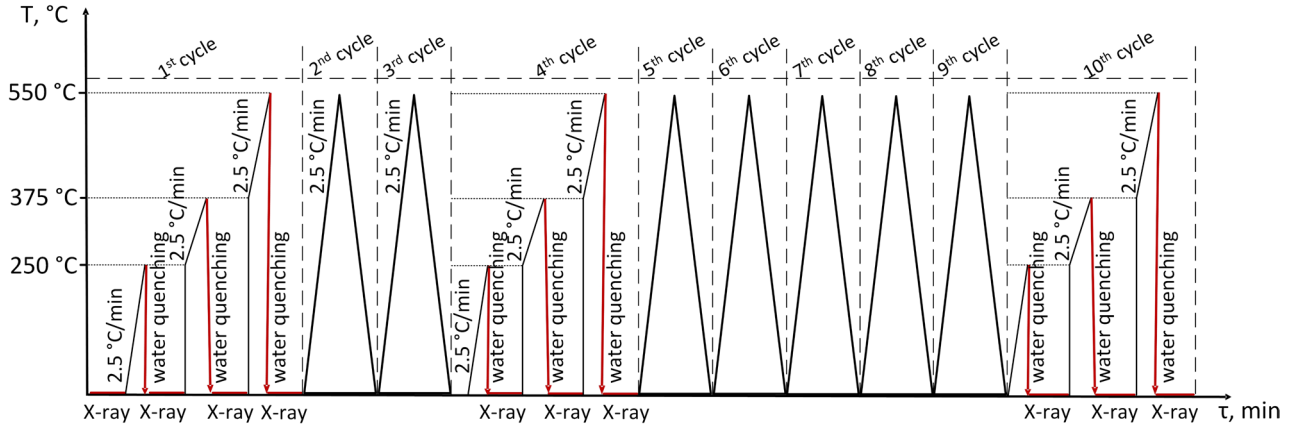

Fig. 1 Sequence of the X-ray diffraction experiment during thermal cycling

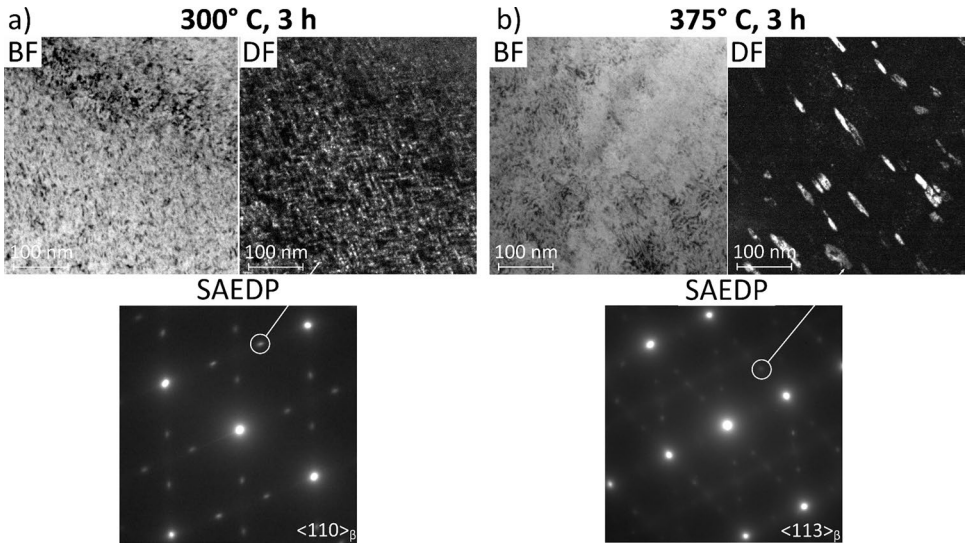

Fig. 2 TEM after aging for 3 h at 300 (**a**) and 375 °C (**b**) of the annealed at 600 °C Ti–22Nb–6Zr SMA: BF—bright field images, DF—dark field images, SAEDP—selected area electron diffraction patterns. DF images are taken from ω-phase reflexes indicated by rings

precipitation, particles are tend to be more equiaxed [40, 41]. The size of the ω_{iso}-phase particles after aging at 300 °C, 3 h is 5…7 × 15…30 nm. Increase of the aging temperature to 375 °C leads to an increase in the ω_{iso}-phase average particle size by about three times.

STEM images of the microstructure at lower and higher magnifications after aging at 300 and 375 °C and the corresponding distribution of local concentrations of Ti, Nb, and Zr elements in the β-phase areas surrounding the ω-phase particle and across this ω-particle is shown in Fig. 3. After aging at 300 °C, the Ti and Nb concentration curves exhibit disordered opposite oscillations along a scanning line (Fig. 3a). These oscillations are observed in the β-phase matrix as well as inside the ω-phase particles. The magnitudes and widths of such oscillations inside the particles do not differ from those observed in the matrix. It means that the ω-phase particles "inherited" the distribution of elements that existed in the β-matrix before the $\beta \rightarrow \omega_{iso}$ transformation without any distinct sign of the element diffusion. On the contrary, distributions of Ti and Nb concentrations scanned after annealing at 375 °C demonstrate clear opposite changes within the ω-phase particle: a peak in Zr concentration and a dip in Nb concentration (Fig. 3b). This corresponds to the expected opposite changes in the concentrations of these elements in the ω-phase particles in the case of their diffusional redistribution in accordance with [32].

Next, the statistical significances of the differences in the distribution of Ti and Nb concentrations (at.%) in the β-phase areas surrounding the ω_{iso}-phase particle and across these ω_{iso}-particles after aging at 300 and 375 °C for 3 h were determined using the Student's test. For this purpose, the whole scanned range was separated into three ranges: I—β-phase matrix "on the left" from the ω-phase particle, II—area across ω-phase particle, III—β-phase matrix "on the right" from the ω-phase particle (Fig. 3). Concentrations of Ti and Nb were averaged over each range separately and over the entire scanned range (I + II + III) after aging at 300 and 375 °C for 3 h (see Table 1).

As can be seen from Table 1, average concentrations of Ti and Nb in the entire (I + II + III) ranges are the same within the error limits after both agings at 300 and 375 °C for 3 h. This means that the whole alloy composition remains stable during aging. For aging at 300 °C, all three ranges (I, II, and III) as well as the entire (I + II + III) range exhibit the same average concentrations of Ti and Nb within the error limits. Therefore, it should be concluded that the there is no statistically significant diffusional element redistribution.

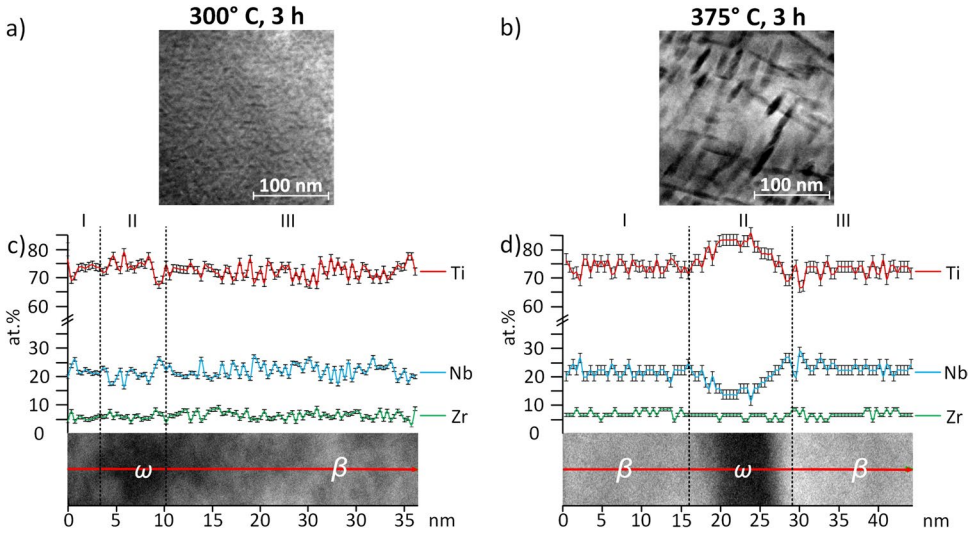

Fig. 3 STEM at lower and higher magnifications after aging for 3 h at 300 (**a**) and 375 °C (**b**) (BF) of the annealed at 600 °C Ti–22Nb–6Zr SMA. The energy dispersive X-ray spectroscopy linear scanning analysis in the area near the ω_{iso}-phase particle after aging for 3 h at 300 (**c**) and 375 °C (**d**)

Table 1 Concentrations of Ti and Nb (at.%) averaged over concentration ranges I, II, III (Fig. 3) separately and over the entire scanned range (I + II + III) after aging at 300 and 375 °C

Aging regime	Element	Entire concentration range (I + II + III)	Concentration range I	Concentration range II	Concentration range III
300 °C, 3 h	Ti	72.08 ± 0.51	72.65 ± 1.70	73.37 ± 1.28	71.72 ± 0.57
	Nb	21.84 ± 0.47	22.17 ± 1.43	20.79 ± 1.13	22.04 ± 0.54
375 °C, 3 h	Ti	70.78 ± 0.77	69.74 ± 0.40	77.45 ± 1.13	68.59 ± 0.75
	Nb	22.29 ± 0.72	23.16 ± 0.37	16.31 ± 1.09	24.62 ± 0.68

After aging at 375 °C, the concentration values in the range I and the entire range (I + II + III) are the same within the error limits. In the range II embracing the ω-phase particle formed, there are large (about 6–7%) increase in Ti and decrease in Nb concentrations, while in the range III, small but statistically significant decrease in Ti and increase in Nb concentrations are observed. It is explained by local diffusional element redistribution which occurs in a local zone of β-phase matrix adjacent to the ω-phase particle on the right (Fig. 3b).

The precision of the applied X-ray spectroscopy technique might seem insufficient to resolve the difference in chemical composition in small ω-phase particles after aging at 300 °C in cases if it is of the same order as or lower than those observed in large ω-phase particles after aging at 375 °C. However, it should be taken into account, that the ω-phase formation manifests C-shape kinetics with maximum rate at 300 °C in the studied alloy, while the ω -phase formation is much slower and weaker at 375 °C [31]. In accordance with [31], the volume fraction of ω-phase after aging at 300 °C is almost three times greater than that after 375 °C. Therefore, if the element diffusion plays the primary role in ω-phase formation, the average changes in the composition after aging at 300 °C should be about three times greater than those observed for 375 °C. Moreover, it should be borne in mind that for the experimental study of the distribution of element concentrations after annealing at different temperatures, ω-phase particles of approximately the same size were selected, and the lengths of the scanning lines from one particle boundary to the other were the same and amounted to 6–7 nm (see Fig. 3a, b). Taking into account the shape of a real C-curve, it seems that the scanning line in Fig. 3b passes through the particle just formed at 375 °C, while the scanning line of the same length passes through the particle exposed to high temperature (300 °C) for a long time. Consequently, the diffusion could not play the leading role in ω-phase formation at 300 °C and plays the secondary role manifested at a higher aging temperature (375 °C).

A comparison of the diffusion mobility of Nb atoms in Ti at temperatures of 300 and 375 °C shows that such a significant difference in the development of the redistribution of Nb atoms at not too large a temperature difference is not something unexpected. To compare the diffusion rates of Nb in β-Ti at 300 and 375 °C, the Nb diffusion coefficients in β–Ti were calculated using the Arrhenius Equation $D = D_o \times e[-E/(R \times T)]$, for which $D_o = 2.91 \times 10^{-8}$ m^2/s and $E = 129.9$ kJ/mol were taken from [42]. The calculations have brought the following results: $D_{Nb} = 4.19 \times 10^{-20}$ and 9.84×10^{-19} m^2/s for 300 and 375 °C, respectively. This means that the diffusion rate of Nb at a temperature of 300 °C is more than 20 times less than at a temperature of 375 °C. This fully correlates with the experimentally observed absence of a significant contribution of the diffusion mechanism to the process of formation of the ω_{iso}-phase at 300 °C.

Study of β→ω_{iso} Transformation Thermocyclic Stability

The study of $\beta \rightarrow \omega_{iso}$ transformation thermocyclic stability was carried out on polygonized and recrystallized structure states of the alloy in order to exclude the influence of crystal lattice defects on this process. The X-ray diffractograms corresponding to quenching from the characteristic temperatures in the 1st, 4th, and 10th cycles in the experiments on thermocyclic stability are shown in Fig. 4a, b. In both P and R structure states, the main phase in the studied temperature range of this alloy is a body-centered cubic (BCC) β-phase. Appearance of the ω_{iso}-phase X-ray diffraction lines is observed after heating to 375 °C during all the studied cycles. Further heating up to 550 °C led to the ω_{iso}-phase disappearance. Such a behavior of ω_{iso}-phase correlates well with the $\beta \rightarrow \omega \rightarrow \beta$ transformation peak in the temperature dependence of square of resonant oscillation frequency f_r^2 upon heating in a torsion pendulum experiment [34]. There was no evidence of any other phase formation.

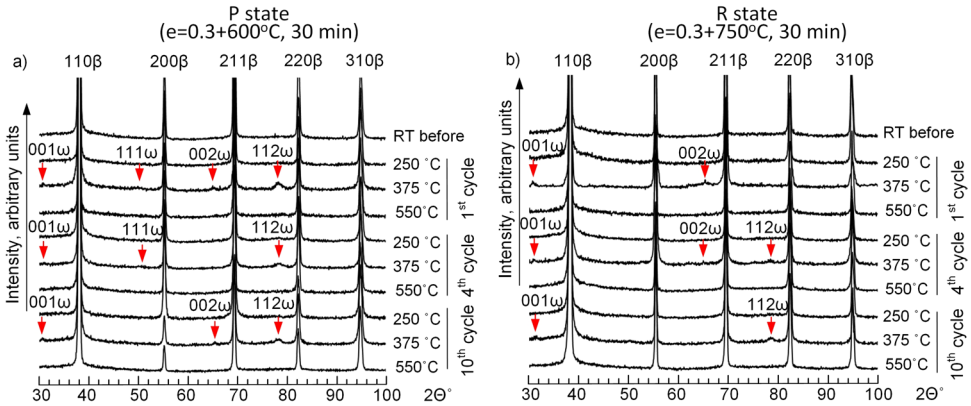

Fig. 4 X-ray diffractograms (**a, b**) in the polygonized (**a**) and recrystallized (**b**) states of Ti-22Nb-6Zr during thermal cycling (at RT after quenching)

For an integral assessment of the stability of β-phase composition upon heating after water-quenching from characteristic temperatures, the β-phase lattice parameter a_β and the half-height width B_{hkl} of $\{110\}_\beta$ and $\{211\}_\beta$ X-ray line profiles were measured at RT (Fig. 5). Figure 5a, b show that the β-phase lattice parameter a_β does not change after quenching from all the characteristic temperatures. This confirms that the observed diffusional element redistribution in the composition of β-phase in Fig. 3 and Table 1 has a local nano-scale nature and does not affect the whole volume of β-phase body during the ω-phase formation. The X-ray line profiles have normal symmetry without a gravity center shift, which confirms the absence of solution inhomogeneity. The B_{hkl} of β-phase does not change, except for certain cases of a slight systematic increase in the B_{211} values after quenching from 375 °C due to the ω_{iso}-phase formation. This increase does not exceed the error limits (Fig. 5c, d). The ω_{iso}-phase lattice parameters a, c, c/a and unit cell volume (Ω) stay unchanged at RT after each heating–cooling cycle (Fig. 6). The calculated c/a of ratio 0.613 ± 0.004 coincides with the previously obtained values for isothermal and athermal ω-phases measured for the Ti–22Nb–6Zr alloy in [31, 39].

It can finally be asserted that the observed formation of ω_{iso}-phase upon heating occurs by the shear mechanism accompanied by the diffusional redistribution of elements only at higher temperatures, and this process is stable and reproducible up to at least ten thermal cycles; the nature of stress fields which accompany the ω-phase formation requires further detailed investigation.

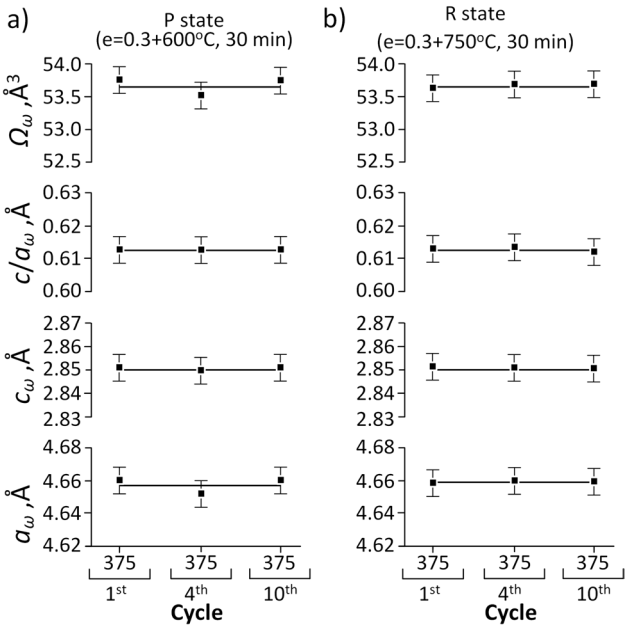

Fig. 6 Lattice parameters of ω_{iso}-phase in polygonized (**a, c**) and recrystallized (**b, d**) states of Ti–22Nb–6Zr SMA during thermal cycling (measured at RT after quenching from 375 °C)

Conclusion

1. The absence of diffusional redistribution of elements across the ω_{iso}/β interfaces and in areas surrounding the ω_{iso}-phase particles was revealed in Ti–22Nb–6Zr SMA at lower aging temperature of 300 °C. This process was observed only at higher temperature of 375 °C. These results indicate that the leading mechanism of the isothermal ω_{iso}-phase formation is a crystal lattice shear, while the diffusional mechanism plays a secondary role

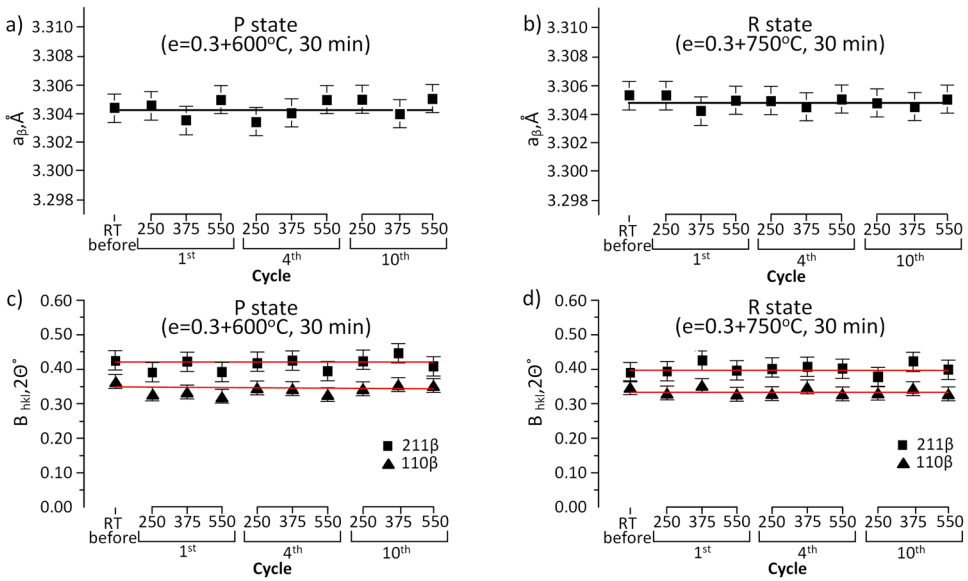

Fig. 5 Lattice parameters a_β (**c, d**) and half-height width B_{hkl} of β-phase X-ray lines (**e, f**) in the polygonized (**a, c, e**) and recrystallized (**b, d, f**) states of Ti–22Nb–6Zr during thermal cycling (at RT after quenching)

which appears only at higher aging temperatures. Its effect is local and does not affect the composition of a main β-phase body in the studied aging conditions. It could take a part in the stress relaxation mechanisms inherent in isothermal shear transformations.

2. The $\beta \rightarrow \omega_{iso}$ transformation features, β- and ω-phases structure parameters during thermal cycling of Ti–22Nb–6Zr SMA are stable and reproducible up to at least 10 thermal cycles. The ω_{iso}-phase and β-phase lattice parameters, β-phase X-ray line width and the amount of the precipitated phase are similar within the error limits after 1st, 4th, and 10th cycles of the ω_{iso}-phase precipitation–dissolution in both polygonized and recrystallized states.

Acknowledgements The present work has been carried out with the financial support of the Russian Science Foundation, project number 23-73-01108, https://rscf.ru/en/project/23-73-01108/ (X-ray diffraction analysis) and the Natural Science and Engineering Research Council of Canada (NSERC) (ingot manufacturing), A.K. is grateful to the Winning Normandy MSCA-co-fund grant (NCBA2LMCO2U) (HSTEM with EDS) and strategic project "Biomedical materials and bioengineering" within the framework of the Strategic Academic Leadership Program "Priority 2030" at NUST "MISIS" (thermomechanical treatment).

Data availability The data that support the fndings of this study are available from the corresponding author upon reasonable request.

References

1. Kim HY, Hashimoto S, Il KJ et al (2004) Mechanical properties and shape memory behavior of Ti-Nb alloys. Mater Trans 45:2443–2448
2. Kuramoto S, Furuta T, Hwang J et al (2006) Elastic properties of gum metal. Mater Sci Eng, A 442:454–457. https://doi.org/10.1016/j.msea.2005.12.089
3. Niinomi M (2008) Mechanical biocompatibilities of titanium alloys for biomedical applications. J Mech Behav Biomed Mater 1:30–42
4. Yoneyama T, Miyazaki ST (2009) Shape memory alloys for biomedical applications. Woodhead Publishing, Philadelphia
5. Biesiekierski A, Wang J, Abdel-Hady Gepreel M, Wen C (2012) A new look at biomedical Ti-based shape memory alloys. Acta Biomater 8:1661–1669
6. Aeby-Gautier E, Settefrati A, Bruneseaux F et al (2013) Isothermal α″ formation in β metastable titanium alloys. J Alloy Compd 577:439–443. https://doi.org/10.1016/j.jallcom.2012.02.046
7. Bönisch M, Calin M, Waitz T et al (2013) Thermal stability and phase transformations of martensitic Ti-Nb alloys. Sci Technol Adv Mater 14:055004. https://doi.org/10.1088/1468-6996/14/5/055004
8. Kim HY, Fu J, Tobe H et al (2015) Crystal structure, transformation strain, and superelastic property of Ti–Nb–Zr and Ti–Nb–Ta Alloys. Shape Memory Superelasticity 1:107–116. https://doi.org/10.1007/s40830-015-0022-3
9. Sheremetyev V, Petrzhik M, Zhukova Y et al (2020) Structural, physical, chemical, and biological surface characterization of thermomechanically treated Ti-Nb-based alloys for bone implants. J Biomed Mater Res Part B Appl Biomater 108:647–662. https://doi.org/10.1002/jbm.b.34419
10. Il KJ, Kim HY, Inamura T et al (2005) Shape memory characteristics of Ti–22Nb–(2–8) Zr (at.%) biomedical alloys. Mater Sci Eng A 403:334–339
11. Kim HY, Ikehara Y, Il KJ et al (2006) Martensitic transformation, shape memory effect and superelasticity of Ti–Nb binary alloys. Acta Mater 54:2419–2429
12. Gasik MM, Yu H (2009) Phase Equilibria and Thermal Behavior of the Biomedical Ti-Nb-Zr Alloy. In Proceedings of the 17th Plansse Seminar, Reutte, Austria
13. Collings EW (1984) The physical metallurgy of titanium alloys. American Society for Metals, US
14. Melton KN (1990) Ni-Ti based shape memory alloys. Engineering aspects of shape memory alloys. Butterworth-Heinemann, London, pp 21–25
15. Otsuka K, Wayman CM (1999) Shape memory materials. Cambridge University Press, UK
16. Miyazaki S, Kim HY, Hosoda H (2006) Development and characterization of Ni-free Ti-base shape memory and superelastic alloys. Mater Sci Eng A 438–440:18–24. https://doi.org/10.1016/j.msea.2006.02.054
17. Prokoshkin SD, Brailovski V, Inaekyan KE et al (2008) Structure and properties of severely cold-rolled and annealed Ti–Ni shape memory alloys. Mater Sci Eng A 481–482:114–118. https://doi.org/10.1016/j.msea.2007.02.150
18. Dubinskiy SM, Prokoshkin SD, Brailovski V et al (2011) Structure formation during thermomechanical processing of Ti-Nb-(Zr, Ta) alloys and the manifestation of the shape-memory effect. Phys Met Metall 112:529–542. https://doi.org/10.1134/S0031918X11050206
19. Inaekyan K, Brailovski V, Prokoshkin S et al (2015) Comparative study of structure formation and mechanical behavior of age-hardened Ti-Nb-Zr and Ti-Nb-Ta shape memory alloys. Mater Charact 103:65–74. https://doi.org/10.1016/j.matchar.2015.03.016
20. Lukashevich KE, Sheremetyev VA, Kudryashova AA et al (2022) Effect of forging temperature on the structure, mechanical and functional properties of superelastic Ti-Zr-Nb bar stock for biomedical applications. Letters on Materials 12:54–58
21. Al-Zain Y, Kim HY, Koyano T et al (2011) Anomalous temperature dependence of the superelastic behavior of Ti–Nb–Mo alloys. Acta Mater 59:1464–1473. https://doi.org/10.1016/j.actamat.2010.11.008
22. Dey GK, Tewari R, Banerjee S et al (2004) Formation of a shock deformation induced ω phase in Zr 20 Nb alloy. Acta Mater 52:5243–5254
23. Rivard J, Brailovski V, Dubinskiy S, Prokoshkin S (2014) Fabrication, morphology and mechanical properties of Ti and metastable Ti-based alloy foams for biomedical applications. Mater Sci Eng C 45:421–433
24. Kreitcberg A, Sheremetyev V, Tsaturyants M et al (2019) Optimization of post-processing annealing conditions of the laser powder bed-fused Ti–18Zr–14Nb shape memory alloy: structure and functional properties. Shape Memory Superelasticity 5:172–181. https://doi.org/10.1007/s40830-019-00218-5
25. Settefrati A, Aeby-Gautier E, Dehmas M et al (2011) Precipitation in a near beta titanium alloy on ageing: influence of heating rate and chemical composition of the beta-metastable phase. Solid State Phenom 172:760–765
26. Lai MJ, Tasan CC, Zhang J et al (2015) Origin of shear induced β to ω transition in Ti–Nb-based alloys. Acta Mater 92:55–63
27. Dubinskiy S, Korotitskiy A, Prokoshkin S, Brailovski V (2016) In situ X-ray diffraction study of athermal and isothermal omega-phase crystal lattice in Ti-Nb-based shape memory alloys. Mater Lett 168:155–157. https://doi.org/10.1016/j.matlet.2016.01.012

28. Afonso C, Aleixo G, Ramirez A, Caram R (2007) Influence of cooling rate on microstructure of Ti–Nb alloy for orthopedic implants. Mater Sci Eng C 27:908–913. https://doi.org/10.1016/j.msec.2006.11.001
29. Williams JC, Hickman BS, Leslie DH (1971) The effect of ternary additions on the decompositon of metastable beta-phase titanium alloys. Metal Trans 2:477–484. https://doi.org/10.1007/BF02663337
30. Zhang Y, Liu Z, Zhao Z et al (2017) Preparation of pure α ″-phase titanium alloys with low moduli via high pressure solution treatment. J Alloy Compd 695:45–51
31. Baranova A, Dubinskiy S, Tabachkova N et al (2022) Kinetic features of the isothermal ω-phase formation in superelastic Ti-Nb-Zr alloys. Mater Lett 325:132820. https://doi.org/10.1016/j.matlet.2022.132820
32. Nag S, Banerjee R, Fraser HL (2009) Intra-granular alpha precipitation in Ti-Nb-Zr-Ta biomedical alloys. J Mater Sci 44:808–815. https://doi.org/10.1007/s10853-008-3148-2
33. Li T, Kent D, Sha G et al (2016) New insights into the phase transformations to isothermal ω and ω-assisted α in near β-Ti alloys. Acta Mater 106:353–366
34. Dubinskiy S, Markova G, Baranova A et al (2022) A non-typical Elinvar effect on cooling of a beta Ti-Nb-Zr alloy. Mater Lett 314:131870. https://doi.org/10.1016/j.matlet.2022.131870
35. Wang K, Wu D, Wang D et al (2022) Influence of cooling rate on ω phase precipitation and deformation mechanism of a novel metastable β titanium alloy. Mater Sci Eng A 829:142151. https://doi.org/10.1016/j.msea.2021.142151
36. Sheremetyev V, Brailovski V, Prokoshkin S et al (2016) Functional fatigue behavior of superelastic beta Ti-22Nb-6Zr(at%) alloy for load-bearing biomedical applications. Mater Sci Eng C 58:935–944. https://doi.org/10.1016/j.msec.2015.09.060
37. Brailovski V, Prokoshkin S, Inaekyan K et al (2012) Mechanical properties of thermomechanically-processed metastable beta Ti-Nb-Zr alloys for biomedical applications. Materials Science Forum. Trans Tech Publications Ltd., Switzerland, pp 455–460
38. Prokoshkin S, Brailovski V, Korotitskiy A et al (2013) Formation of nanostructures in thermomechanically-treated Ti-Ni and Ti-Nb-(Zr, Ta) SMAs and their roles in martensite crystal lattice changes and mechanical behavior. J Alloy Compd 577:418–422. https://doi.org/10.1016/j.jallcom.2011.12.153
39. Dubinskiy S, Prokoshkin S, Brailovski V et al (2014) In situ X-ray diffraction strain-controlled study of Ti-Nb-Zr and Ti-Nb-Ta shape memory alloys: crystal lattice and transformation features. Mater Charact 88:127–142. https://doi.org/10.1016/j.matchar.2013.12.008
40. Williams JC, Hickman BS, Marcus HL (1971) The effect of omega phase on the mechanical properties of titanium alloys. Metal Trans 2:1913–1919
41. Hickman BS (1969) Omega phase precipitation in alloys of titanium with transition metals. In: North American Rockwell Corp. North American Rockwell Corp, Thousand Oaks
42. Bakker H, Bonzel HP, Brugg AM, Dayananda MA, Gust W, Horvath J, Kaur I, Kidson GV, LeClaire AD, Mehrer H, Murch GE, Neumann N, Stolica G, Stolwijk NA (1990) Diffusion in solid metals and alloys / Diffusion in festen Metallen und Legierungen. Springer, Cham.